Heliyon 6 (2020) e05840

Contents lists available at ScienceDirect

Heliyon

journal homepage: www.cell.com/heliyon

Research article

Simulation and optimization of a lamella settler for cattle feedlot wastewater treatment and nutrients recovery. Experimental validation in the field

Santiago N. Fleite [a,b], Ana R. García [b], Christian De los Santos [b], Leandro L. Missoni [d,e], Rocío Torres [d], M. Gabriela Lagorio [d,e], Miryan Cassanello [a,c,*]

[a] Universidad de Buenos Aires, Facultad de Ciencias Exactas y Naturales, Dpto. Industrias, LARSI, Ciudad Universitaria, C1428BGA, Buenos Aires, Argentina
[b] Cátedra de Química Inorgánica y Analítica, Facultad de Agronomía, Universidad de Buenos Aires, Argentina
[c] CONICET, Universidad de Buenos Aires, Instituto de Tecnología de Alimentos y Procesos Químicos (ITAPROQ), Facultad de Ciencias Exactas y Naturales, Buenos Aires, Argentina
[d] CONICET, Universidad de Buenos Aires, INQUIMAE, Facultad de Ciencias Exactas y Naturales, Buenos Aires, Argentina
[e] Universidad de Buenos Aires, Facultad de Ciencias Exactas y Naturales, Dpto. de Química Inorgánica, Analítica y Química Física, Ciudad Universitaria. Pabellón II, 1er piso, C1428EHA, Buenos Aires, Argentina

ARTICLE INFO

Keywords:
Cattle feedlot wastewater treatment
Lamella settler
Particle settling
Effluent characterization
CFD optimization
Feedlot effluent spectral analysis

ABSTRACT

Cattle concentrated animal feeding operations (feedlots), whose number has grown considerably in the last years, generate large volumes of wastewaters with a high organic load. The wastewaters are formed by rainfall-runoff of the accumulated manure and may contain hormones and antibiotics, which hampers the use of biological treatments. In this work, the feasibility of continuous separation of the suspended colloidal organic matter and nutrients to clarify the liquid and recover the solid is studied. A flocculation sedimentation system using a decentralized lamella settler is proposed, optimized and further tested in the field. Computational fluid dynamic (CFD) simulation is used to analyze the motion of the liquid and suspended inertial particles representing the formed flocs, for optimizing the settler. The simulations helped in the design of the bench-scale unit tested in the field. The clarified liquid was characterized to analyze its use for fertigation. The proposed treatment allowed excellent removal of organic matter (~98% chemical oxygen demand, and almost complete turbidity) and phosphorus (~95%). Organic nitrogen was partially removed (~70%) and ammonia nitrogen mostly remained in the liquid. Spectral characterization of the clarified liquid suggests that the remaining organic nitrogen is related to soluble protein-like compounds.

1. Introduction

Cattle concentrated animal feeding operations (feedlots) are among the most important agricultural systems, and the number of establishments has readily increased in the last twenty years. Since feedlots involve high animal density in confined growth, the excreta form large manure accumulations. During rains, runoff mixed with surface manure produces highly polluted wastewaters, which are typically stored in accumulation ponds. These wastewaters contain a large amount of labile organic matter, nutrients (K, N and P mainly) and salts, minor constituents such as metals (Cu, Zn, and Fe) and organic compounds (antibiotics, hormones and other ionophores), as well as pathogens (Giardia, Escherichia coli) (García et al., 2013). These agents can be mobilized by water dynamics and reach superficial or subsurface water sources, degrading their quality (García et al., 2012). Despite biological treatments have been widely used for other animal productions (Hjorth et al., 2010), there are disadvantages in applying these technologies in cattle feedlots. Since the wastewater is produced by rainfall-runoff, the discontinuous and unpredictable characteristics of the generation prevent its continuous use as a substrate for bioprocesses. Moreover, the presence of hormones, antibiotics resistant bacteria, and especially the antibiotics existing in the wastewater (Jahne et al., 2014) leads to drawbacks for sustaining a biological treatment system.

Apart from the relevance of rapid control of the pollution risk after copious rains, recovering the nutrients and organic matter from the wastewaters to develop a solid fertilizer would be profitable for the

* Corresponding author.
E-mail address: miryan@di.fcen.uba.ar (M. Cassanello).

https://doi.org/10.1016/j.heliyon.2020.e05840
Received 10 September 2020; Received in revised form 21 November 2020; Accepted 21 December 2020

agricultural production. For this, a treatment system that allows efficient and fast recovery of the nutrients and organic matter is required. Settling is a well-known wastewater treatment operation that allows rapid treatment and efficient separation of the organics. It involves the separation of the suspended solids by gravitational forces. If the water contains suspended colloidal solids, coagulation-flocculation is used to assist the precipitation. Settling has been largely applied for urban sludge and other wastewaters (Xue et al., 2018), although for agricultural systems, and particularly feedlots, it has been less assessed. Pepple et al. (Pepple et al., 2011) studied the settling properties of a raw feedlot wastewater. They found that a large fraction of the solids settled rapidly and was easily separated in an accumulation pond. Nevertheless, the nitrogen, phosphorus and organic matter concentrations in the ponds were still quite above the limits allowed for discharge. Fleite et al. (2020) evidenced the feasibility of continuous separation of suspended colloidal solids from feedlot wastewater by promoting the coagulation-flocculation in a Koflo type static mixer. Almost complete recovery of the nutrients and suspended organic matter was attained due to the improved settling features of the formed flocs. Hence, the use of an efficient settler to recover the solid formed by continuous coagulation-flocculation from the feedlot wastewaters would allow rapid treatment and eventual development of a solid fertilizer (Ciapparelli et al., 2016), while the clarified water may be used for fertigation (Delin and Stenberg, 2020).

Among possible settler designs, lamella settlers are considered as the best high rate low-cost settling systems available. The achievable settling efficiency allows using units smaller than conventional settlers or sedimentation basins (Getaz, 2018). Lamella settlers have been used for many applications as secondary clarifiers (Tchobanoglous et al., 2014a, b), stormwater treatment (Fuchs et al., 2013; Weiss, 2013), dairy wastewater treatment (Martín-Rilo et al., 2015), and other food industry installations (Getaz, 2018). Despite many applications of lamella settlers, optimization for treating the feedlot wastewater would lead to better performance. Optimization generally relies in simulations validated with experimental evidence. Computational fluid dynamic (CFD) simulations of lamella packs (Shen and Yanagimachi, 2011), simplified lamella type flow systems (Salem et al., 2011) and rectangular settling tanks with lamella packs (Tarpagkou and Pantokratoras, 2014) have been reported. Packed-lamella settlers, often used for enhanced sedimentation basins, have also been analyzed (Takata and Kurose, 2017). Other configurations of lamella settlers are under research, including decentralized systems for runoff treatment (Fettig et al., 2017). Scarce information is available regarding a complete analysis of both the fluid flow and solids behavior, and about the flow path influence on the lamella performance. Al-Sammarraee et al. (2009) evidenced that small particles tend to move following fluid paths, hence reaching the entire settler volume, while bigger particles settle near the inlet. Therefore, optimization cannot rely only on fluid dynamics, it requires considering the combined effect of particles and fluid for a correct assessment.

Experiments evidencing the continuous operation of pilot-scale settling equipment are scarce, particularly for feedlots. Hence, the objective of this work is to develop an optimized decentralized lamella settler coupled with an inflow coagulation-flocculation system useful for treating cattle feedlot wastewater. The pilot unit was optimized using CFD simulations, and the prototype was tested in the field. Results of both stages are included in the work.

2. Materials and methods

2.1. Computational fluid dynamics (CFD)

Simulations were performed using the Gerris Flow Solver CFD open-source software (Popinet, 2003) in a 2D arrangement. Gerris has been applied to interpret the underlying dynamics of multiphase flows and phases interactions in several systems (Keen et al., 2013; Salvador et al., 2016; Shui et al., 2015). In this study, the simulation of the liquid and flocs motion in the lamellar settler was carried out using the incompressible fluid Navier-Stokes DNS solver with an octree data structure for mashing (Lagrée et al., 2011; Popinet, 2003), in a two-dimensional arrangement ($U_z = 0$).

$$\nabla \cdot \mathbf{U} = 0 \tag{1a}$$

$$\rho\left[\frac{\partial \mathbf{U}}{\partial t} + (\mathbf{U}\cdot\nabla)\mathbf{U}\right] = -\nabla P + \mu\nabla^2\mathbf{U} \tag{1b}$$

Where $\mathbf{U}$ is the velocity vector, P the fluid pressure, and μ the dynamic viscosity.

Concerning the boundary conditions, a Dirichlet no-slip condition was set for the velocity in all solid-liquid boundaries. At the fluid inlet, the boundary condition was a Dirichlet with velocity value equal to the inlet fluid velocity. At the outflow, a Dirichlet condition was used for the pressure ($P = 0$) and a Neumann condition was set for the vertical velocity ($U_y = 0$).

Apart from the velocity fields and kinetic energy distribution, results allowed obtaining the residence time distribution (RTD) of an ideal tracer injected as a step function, following the scalar variable tracer technique as described by O'Callaghan et al. (O'Callaghan et al., 2010). Moreover, validation of CFD analysis was achieved by comparing experimental RTD curves determined in the built pilot-scale lamella settler with the simulated ones, as recommended by Salem et al. (2011). After validation and optimization using the liquid RTD curves, the motion of inertial particles, representing the flocs formed by coagulation, was simulated following Tomar et al. (2010), with a single 200 particles injection in the inflow zone, linearly distributed along the *y*-direction, to characterize the settler performance. All particles were spherical with diameter equal to ⅕ of the inlet diameter. They behaved independently of each other without disturbing the fluid motion. Their density was calculated from a submerged object forces balance using the initial settling velocity measured for coagulated feedlot wastewater reported in Fleite et al. (2020). The resulting value for the density of the particles (ρ_p) was 1001.81 kg m^{-3}.

$$\rho_p = \rho_L \cdot \left(\frac{3}{4}\cdot\frac{C_D V_s^2}{g d_p} + 1\right) \tag{2}$$

Where V_s is the settling velocity for the coagulated feedlot wastewater, g is the gravitational acceleration, d_p is the particle diameter, and ρ_L, ρ_p are the liquid (1000 kg m^{-3}) and particles' densities, respectively. The drag coefficient, C_D, was calculated following the Brown and Lawler correlation (Brown Phillip, P. and Lawler Desmond, 2003) (Eq. 3).

$$C_D = \frac{24}{Re_p}\cdot\left(1 + 0.15Re_p^{0.681}\right) + \frac{0.407}{1+\frac{8710}{Re_p}} \quad Re_p < 2\cdot 10^5 \tag{3a}$$

Where Re_p is the Reynolds number for the particle defined as in Eq. (3b).

$$Re_p = \frac{d_p V_s \rho_L}{\mu} \tag{3b}$$

The tested geometries are schematized in Figure 1. First, a rectangular sedimentation tank (Figure 1a) was simulated. Then, modifications were included, leading to the following configurations: a tank with a 0.25 m height baffle located at 0.1 m from the left boundary, horizontally aligned with the inlet tube (Figure 1b), a structure with bottom inclinations without lamellas (V-shape, Figure 1c), the structure shown in Figure 1c provided with the front lamella (Figure 1d), a complete lamella settler (Figure 1e), three complete lamella settlers with 0.08 m height inlet baffles with 30° (Figure 1f), 45° (Figure 1g) and 60° (Figure 1h) inclinations, located 0.1 m from the left boundary and horizontally aligned with the inlet tube. Finally, based on the CFD results, the physical prototype was designed, constructed and tested, as described in the next section. Figure 2 illustrates the dimensions used for the 2D simulations.

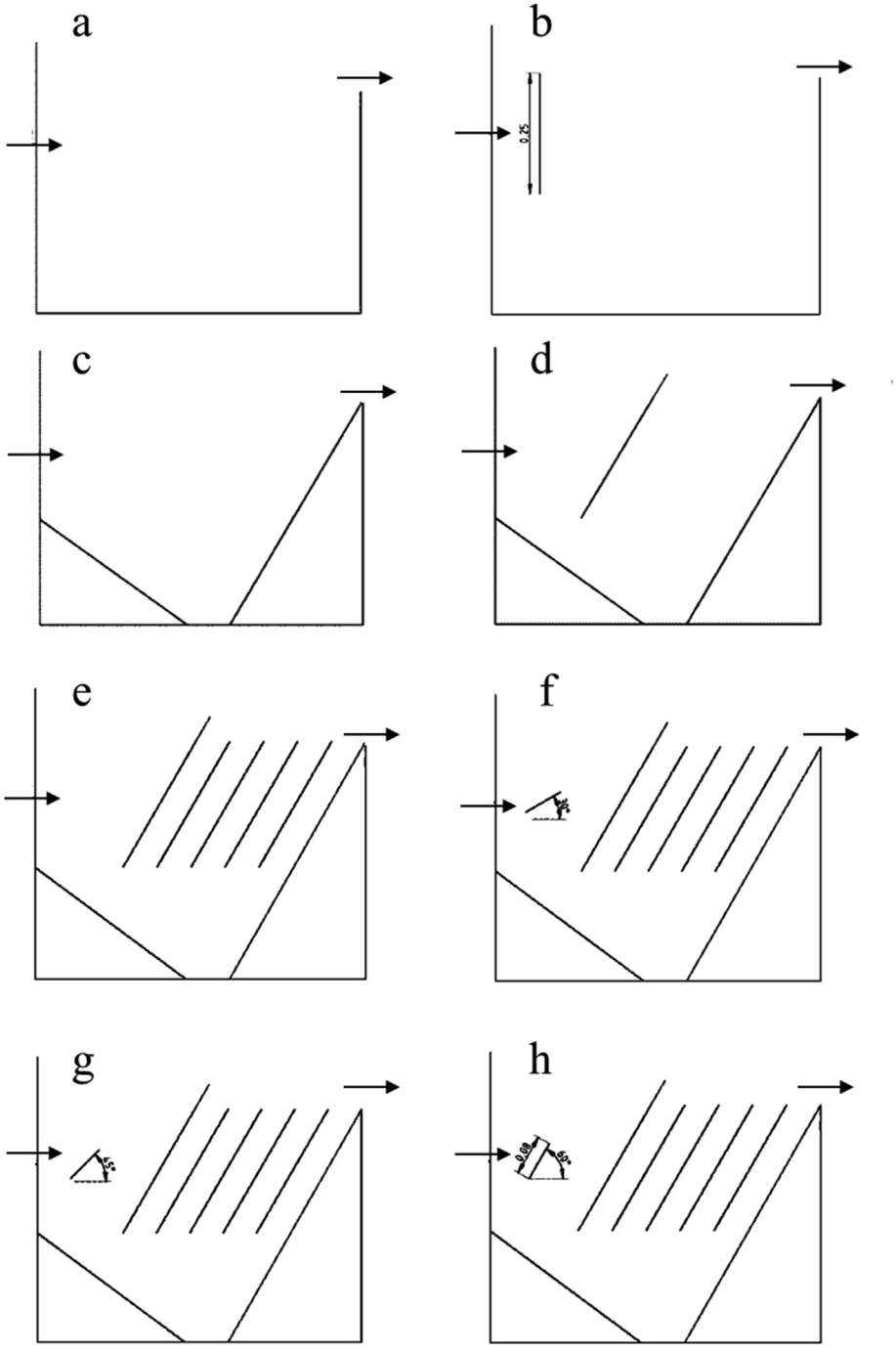

Figure 1. Geometries tested by CFD in the process of optimization. In b, the vertical baffle height is 0.25 m, while in f, g and h, the baffle length is 0.08 m, and its placement angle is 30°, 45°, and 60°, respectively.

2.2. Design of the pilot-scale lamella settler prototype

Results from the CFD analysis were considered to build the pilot-scale unit. Wastewater settling properties considered were those obtained by Fleite et al. (2020) when the coagulation-flocculation was continuously induced in a Koflo type static mixer. The hydraulic retention time was set to fit 2 L min^{-1} flow rate with a final volumetric solid percentage of 25% after coagulation and a 20-minutes settling. The scale factor was 1:100 to the real equipment that would be required for the treatment of a single reservoir pond of approximately 14000 m^3. One such pond existed in the feedlot were the prototype was tested. The pond was intended for 5 days of continuous functioning, which is the half rain average recurrence time for the region. Lamella plates inclination was fixed at 60° as it is widely accepted to be the optimal (Tchobanoglous et al., 2014a,b). The prototype settler width was set in 0.20 m to build the unit used for the experiments. Other dimensions have been given in Figure 2.

2.3. Residence time distribution curves from experiments and simulations

Residence time distribution (RTD) curves of the liquid phase (experiments without solids) were obtained in the built prototype using a potassium chloride solution (KCl, 90 mg L^{-1}) as tracer. Experimental RTD curves were repeated at least three times to assess their reproducibility. The curves were analyzed to determine the parameters used to

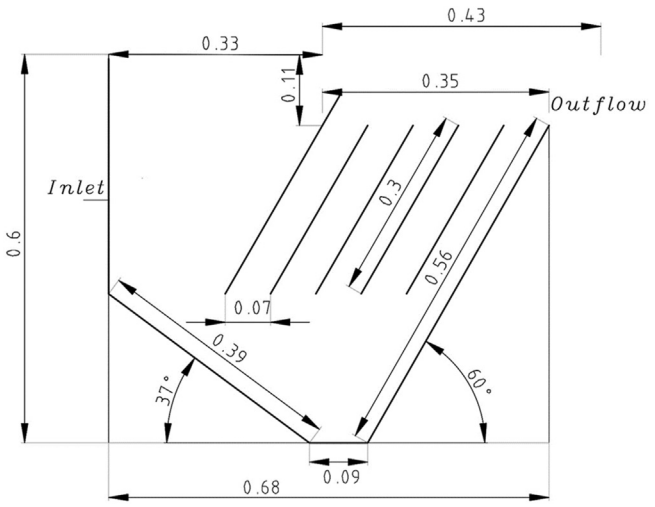

Figure 2. Dimensions (m) used for the 2D simulations, and of the settler pilot unit built for the experiments.

characterize the fluidynamics within the settler and the reported values are the mean of the three independent experiments. RTD curves were used to further validate CFD simulations as previously mentioned. Samples were taken from the settler liquid outflow every 2 min. The injection was a step signal, from which the $F(t)$ function was determined, as expressed in Eq. (4), where $C(t)$ is the tracer concentration in the outlet at time t, and C_{step} its concentration in the injected solution.

$$F(t) = \frac{C(t)}{C_{step}} \tag{4}$$

The experimental cumulated RTD curve ($F(t)$) was used to get the $E(t)$ curve by differentiation. Then, the experimental mean residence time of the liquid (τ) and the dimensionless variance ($\sigma^2{}_\theta$) were determined from the first and second moments, respectively, considering the density function $E(t)$. The same analysis was performed on simulated RTD curves obtained with the Gerris flow solver software.

For mixing assessment, the dimensionless variance ($\sigma^2{}_\theta$) and the Morril index (Mo), defined by Eq. (5), were used (Guo et al., 2015; Teixeira and do Nascimento Siqueira, 2008).

$$Mo = \frac{t_{90}}{t_{10}} \tag{5}$$

Where t_{10} and t_{90} are the times when 10% and 90% of tracer mass has, respectively, left the system. Like the experimental mean residence time (τ), t_{10} and t_{90} can be adimensionalized with the expected mean residence time (T) calculated as the ratio of the settler volume and the liquid flow rate, to get the dimensionless values (θ_m, θ_{10}, θ_{90}). Mo index has low statistical variability and has been recommended for intermediate to well-mixed systems (Teixeira and do Nascimento Siqueira, 2008). Another important information provided by RTD curves is the degree of short-circuiting. Its presence tends to decrease particles residence time in the settler, leading to a diminished probability of settling. The short-circuiting degree was determined using the θ_{10} (Teixeira and do Nascimento Siqueira, 2008).

2.4. Settling performance index (SPI)

Many optimization analyses were based on RTD information to estimate the degree of mixing and short-circuiting (Teixeira and do Nascimento Siqueira, 2008; Tsai et al., 2012). Newer approaches still rely on this kind of information for efficiency analysis, usually combined with particle velocimetry and concentration profiles (Arendze and Sibiya, 2016; Wahl et al., 2010; Wilson and Venayagamoorthy, 2010). Nevertheless, RTD experiments and CFD simulation of the liquid motion do not allow evaluation of the settling efficiency. Then, for comparing settlers with different geometries, information of flocs motion is important. For this purpose, the motion of 200 injected inertial particles have been simulated by CFD to calculate a particle settling efficiency index (SPI) as follows. Let ($P(t)$) be the function that describes the number of particles settled; that is, the ones that have reached the settler bottom or walls and remained there (as defined in (Vahidifar et al., 2018)). A settling factor (α) indicating the settling rate efficiency achieved by the settler can be defined by Eq. (6).

$$\alpha = 1 - \frac{\int_0^{t_{max}} (P_{tot} - P(t))}{P_{tot} t_{max}} \tag{6}$$

Where P_{tot} is the number of particles injected and t_{max} is the time when all the particles have either settled or escaped from the settler. Then, a retention factor (β), accounting for the settler capacity of avoiding solid loses, can be defined by Eq. (7).

$$\beta = 1 - \frac{P_{es}}{P_{tot}} \tag{7}$$

Where (P_{es}) is the total cumulated number of particles that escaped from the settler.

Both α and β will take values between 0 and 1. The closer they are to 1, the better the settler performance. Combining these factors, the settling performance index (SPI) is calculated as expressed in Eq. (8).

$$SPI\% = 100 \cdot \frac{(\alpha + 1) \cdot \beta}{2} \tag{8}$$

SPI is also bounded between 0 and 1. The SPI index increase as the settler performance improves. Table 1 shows a comparison of extreme situations to illustrate index behavior.

2.5. Field experiment and characterizations

Figure 3 shows a schematic of the experimental installation. The inflow system consisted of a floating suction assembly connected to a centrifugal pump through a plastic hose. A diaphragm valve and a rotameter were used to regulate the flow rate. The coagulation-flocculation process was described in Fleite et al. (2020). Briefly, iron chloride and calcium hydroxide solutions were mixed with the wastewater using two peristaltic pumps, with flow rates adjusted to attained 10 mM Fe^{3+} and 15 mM Ca^{2+} final doses. The mixing was accomplished using two Koflo type static mixers located after the injection of each coagulant.

The field experiment was carried out in a cattle feedlot establishment near Marcos Paz city, in Buenos Aires province, Argentina. The installation comprised 91.000 m^2 of earthen pens with runoff collecting

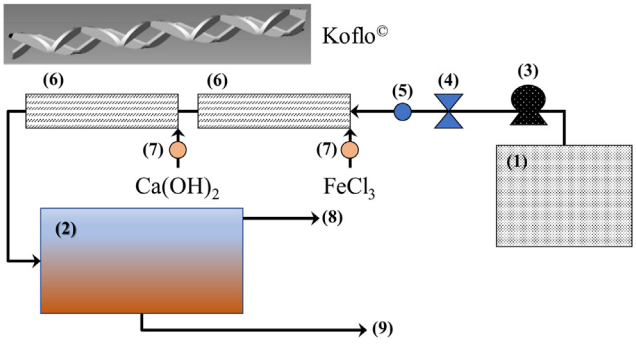

Figure 3. Flowsheet of the coagulation-flocculation-sedimentation experimental system. 1-reservoir pond; 2-settler; 3-centrifugal pump; 4-diaphragm valve; 5-flow meter; 6-static mixers; 7-peristaltic pumps, 8-liquid outflow; 9-solid concentrated outflow.

Table 1. Different situations of a settler performance and SPI expected values.

MEAN SETTLING CONDITION	ESCAPING PARTICLES	α	β	*SPI*
SLOW SETTLING	A lot	0.1	0.1	5.5%
SLOW SETTLING	Few	0.1	0.9	49.5%
FAST SETTLING	A lot	0.9	0.1	9.5%
FAST SETTLING	Few	0.9	0.9	85.5%

channels and a final reservoir pond. The region has a temperate annual regime with an average annual rainfall of around 1000 mm (García et al., 2013).

Standard methods (APHA, 2017) were used for measuring EC (electrical conductivity), pH, ammonia (N–NH_4), total Kjeldahl nitrogen (TKN), total reactive phosphate (TRP), total phosphorus (TP), sodium (Na^+), potassium (K^+), chemical oxygen demand (COD), turbidity (NTU), hardness (Hrd), and alkalinity (Alk). Organic fractions of nitrogen (N-Org) and phosphorus (P-Org) were obtained by difference with totals. All determinations were performed at least three times and the reported values are the mean of the determinations. From the measured values, removal efficiencies (η) were calculated as proposed by Okoth et al. (2008) (Eq. 9).

$$\eta = 100 \cdot \frac{C_{in} - C_{out}}{C_{in}} \tag{9}$$

Where C_{out} and C_{in} are the outlet and inlet concentrations of each measured compound. For soil discharge assessment the sodium adsorption ratio (SAR) was determined (Halliwell et al., 2001) (Eq. 10).

$$SAR = \frac{[Na^+]}{\sqrt{\frac{[Ca^+]+[Mg^+]}{2}}} \tag{10}$$

Where sodium [Na^+], Calcium [Ca^{2+}] and Magnesium [Mg^{2+}] concentrations are expressed as $mmol_c\ L^{-1}$ or mEq L^{-1}.

The untreated and treated wastewater were also analyzed spectroscopically, to get the UV-Vis absorption spectra and the excitation-emission fluorescence matrices (EEMs). Since the conformation of many organic molecules changes with pH, it has been suggested (Zhang et al., 2011) that a good practice to get reliable spectral information is to measure all the samples at the same pH. For this reason, a 0.1 M sodium bicarbonate ($NaHCO_3$) buffer was added to every sample for attaining pH = 8.3 (Zhang et al., 2011).

UV-Visible spectra were measured from 200 nm to 600 nm. From the spectra, characteristics absorbance indices were determined and analyzed following standard considerations (Coble et al., 2014; Waldrip et al., 2014; Zhang et al., 2011). Determined indices, which are ratios of absorbance at given wavelengths, helped interpreting the degree of aromaticity and the average molecular size of the organic matter present in the wastewaters. The absorbance at 254 nm and 272 nm were analyzed since they are also related to the average aromaticity of the

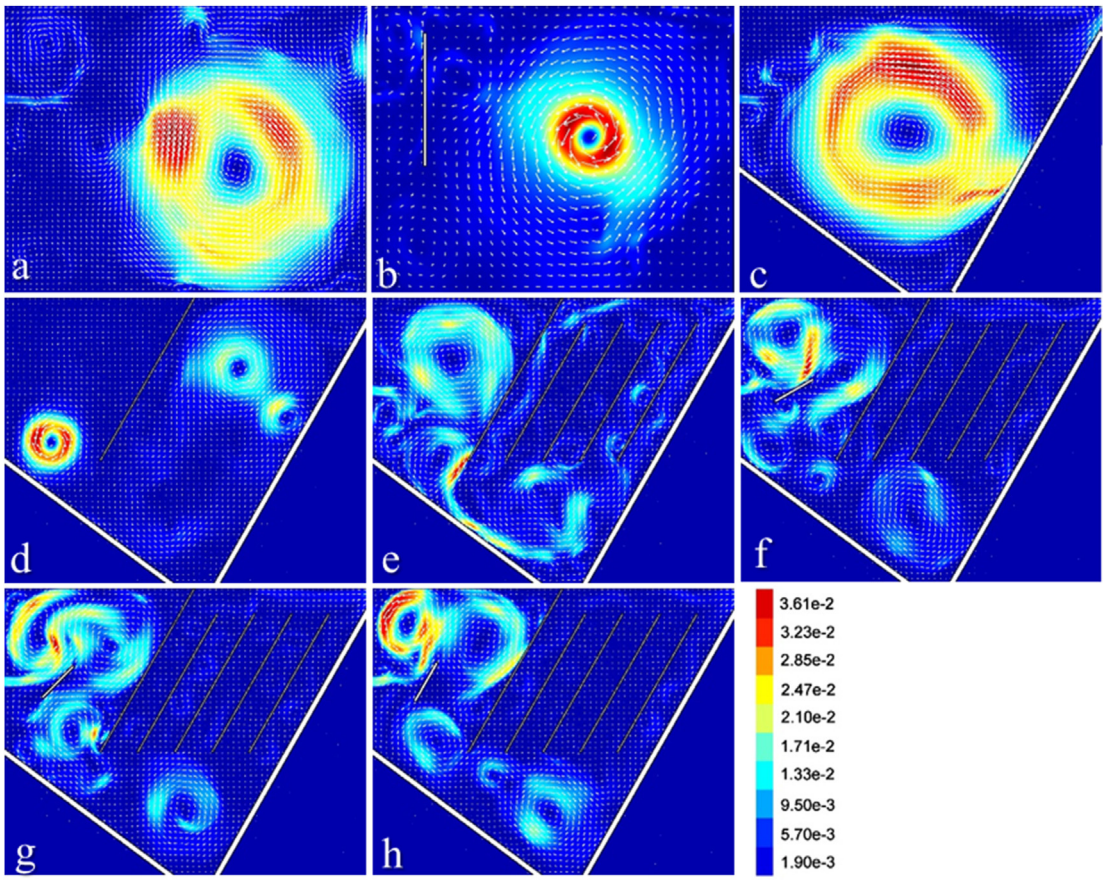

Figure 4. Kinetic energy (J kg^{-1}) and velocity field for the different geometries. Each frame is 0.6 m tall and 0.68 m long. Letters (a–h) correspond to configurations shown in Figure 1.

organic matter; and at 285 nm, where the average absorption peak of humic substances is located (Zhang et al., 2011).

Regarding the fluorescence measurements, excitation-emission measurements were performed to obtain the corresponding matrices (EEMs). This technique provides further detail on the compositional changes of organic matter than the analysis of UV-Vis spectra (Coble et al., 2014). It allows inferring certain characteristics of organic matter such as aromaticity, the type and degree of substitutions (phenolic, carboxylic, etc.), and the presence of certain fluorophores.

Both UV-Vis and fluorescence samples were recorded using 1 cm optical path quartz cuvettes with four transparent windows. Fluorescence measurements were performed by means of a steady-state spectrofluorometer (QuantaMaster, PTI – Photon Technology International) with excitation and emission slit widths set to 4 nm. Excitation-emission matrices were obtained by varying excitation wavelength from 250 nm to 490 nm (in 20 nm intervals), while emission spectra were registered (in steps of 1 nm) from the excitation wavelength +10 nm–600 nm. Emission was corrected by the detector response to different wavelengths by using the correction function included in the instrument software (PTI FelixGX). The general registration, correction and interpretation were carried out following the recommendations of Coble et al. (2014). In all cases, the samples were filtered (0.45 μm) to guarantee the absence of dispersion that could affect the measurements. Afterwards, they were diluted to have absorbance <0.3 at 260 nm for minimizing inner-filtering effects, as suggested in the literature (Ohno and He, 2011). The SpectraGryph 1.2 (Menges, 2020) software was used to remove the Raleigh and Raman peaks from all fluorescence spectra.

3. Results and discussion

3.1. Optimization by CFD

CFD results of velocity fields and kinetic energy obtained for all the studied geometries are shown in Figure 4. CFD analysis indicated a considerable decrease in eddy size and kinetic energy when at least a front baffle was inserted. This effect was observed for the rectangular and V-shape geometries (Figure 4 a-d). The big central eddy of the empty tanks was effectively disrupted by the lamellas, producing a lot of minor eddies with significantly less kinetic energy. When the lamellas were inserted, the localized eddies were less strong, despite the existence of an important turbulent region in the entrance zone. Inclusion of an extra baffle close to the liquid inlet, whatever its inclination, apparently did not lead to further improvement, since the flow paths showed little difference compared to the system without an entrance baffle (Figure 4 e-h).

To further compare the suitability of the different geometries, residence time distribution (RTD) curves have been obtained from the CFD simulations. Figure 5 compares parameters calculated from the curves, indicating the uncertainty in the determinations that arise from the discretization and curve analysis procedure. Parameters calculated from the RTD curves depended significantly on the system geometry. The liquid residence time (θ_m) was higher for geometries with an inclined base (V-shaped, Figure 5 c-h), suggesting a better flow path than in rectangular tanks. Hence, the bottom inclination would be favorable for improving settler efficiency while allowing easy cleaning. The mixing degree, evaluated either by *Mo* or the dimensionless variance, was maximum when neither baffles nor lamellas were present (Figure 5 a, c). It markedly decreased when the entrance baffles were inserted. Configuration with lamellas and no entrance baffle generated slightly higher mixing (Figure 5 e). However, mixing is not necessarily a drawback, it can be beneficial to capture suspended solids. A certain degree of mixing can lead to better performance if it arises from the presence of recirculation zones distributed throughout the settler volume with eddies of low strength (Vahidifar et al., 2018). The configurations without baffles and lamellas also led to the highest short-circuiting, indicated by the lowest values of θ_{10}. Insertion of an entrance baffle decreased the short-circuiting probably by interfering with the mayor circulation path. The presence of lamellas also decreased the degree of short-circuiting. The configurations with lamellas provided with an extra baffle close to the liquid inlet resulted in lower values of θ_{10}. He et al. (He et al. (2018)) have argued that baffles could increase the short-circuiting due to higher inlet speeds. Inspection of the CFD simulations shown in Figure 4 (f-h) indicated that the entrance baffles in the lamella settler resulted in higher kinetic energy around the inlet zone, in coincidence with the lower values of θ_{10}. The configuration showed in Figure 1 e, with the V-shape walls, filled with lamellas and with no entrance baffle resulted in the best option, so it was selected to build the prototype.

3.2. CFD validation from RTD curves

After building the experimental unit, the simulation was validated by comparing RTDs of the liquid obtained with the Gerris code and in the experimental setup, for three geometries (Figure 6). The simulation was able to satisfactorily predict the experimental curves for the three tested geometries. Liquid residence times, τ, calculated from the simulated curves agreed with the experimental data, with relative errors of around 2 % (Table 2), further indicating the ability of the simulation to represent the experimental results.

3.3. Particle settling efficiency index

For comparing the solid separation efficiency of the different geometries, the motion of 200 injected inertial particles have been simulated by CFD (Figure 7), as explained before.

The comparison was made in terms of the particle settling efficiency index (*SPI*) defined in Eq. (8). Calculated values of the α, β and *SPI* index for the studied geometries are given in Table 3. The standard deviation of the index has been estimated by repeating the simulation of the 200 particles trajectories starting from different randomly taken initial positions.

As observed in the table and in Figure 7, almost all the tested geometries had excellent performance regarding particles retention (β), except the rectangular tank without baffles. However, the settling efficiency (α) showed significant dependence on settler geometry. The empty tanks, either rectangular (Figure 1 a and 7 a) or V-shaped (Figure 1 c and 7 c) had the worse results, but their performance in terms of particle settling largely improved by adding a frontal baffle (Figure 1 b, d and 7 b, d). Lamella systems resulted in much-improved settling efficiency. The chosen configuration for building the set-up (Figure 2 and Figure 7 e) showed the best performance. Insertion of an entrance baffle, despite not affecting the excellent retention features (Figure 1 f-h and 7 f-h), reduced the settling efficiency likely due to the increased turbulence and velocity in the entrance region (see Figure 4 f-h). This result agrees with those reported in (He et al., 2018), who argued that baffles can decrease the

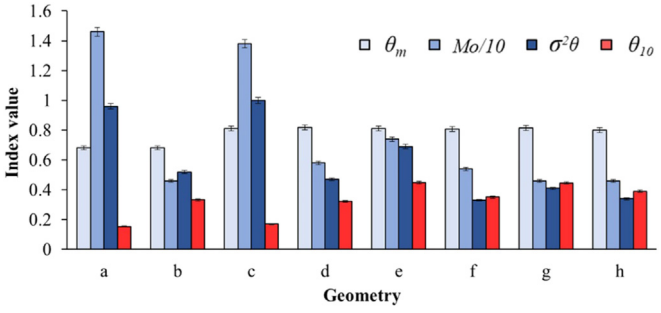

Figure 5. Liquid mean residence time and indexes used to estimate the degree of mixing (blue) and short-circuiting (red) determined from RTD curves. Morril index values (Mo) are shown divided by ten to facilitate their comparison with the other indexes. Letters (a–h) correspond to configurations shown in Figure 1. Error bars indicate the uncertainty in parameter estimation from the simulated RTD curves.

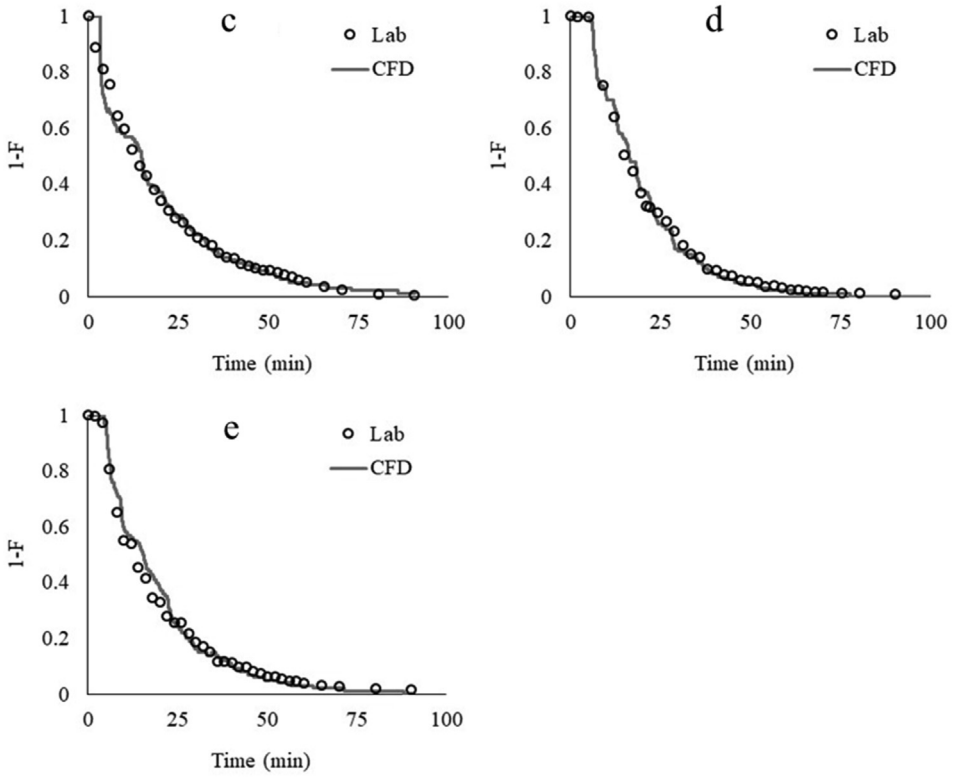

Figure 6. Comparison of experimental liquid RTD curves with those obtained from CFD simulation. Configurations correspond to those shown in Figure 1 c, d and e.

settling performance if turbulence is increased. While this was attributed mainly to floc breakage (He et al., 2018), the simulation of the inertial particles motion (Figure 7) indicated that the entrance baffles also led to a worse settling behavior.

3.4. Field experiment with continuous operation

3.4.1. Chemical composition

The field experiment was carried out in continuous mode using the lamella settler prototype that was built based on the optimization results (Figure 2). Figure 8 depicts the results of the main variables removal efficiency, for a representative period of time during the continuous field experiment (one sample every minute for around an hour). Although concentrations were determined by triplicate and the efficiency was calculated from the mean, the error of reproducibility for each sample was far below the variability among the samples. We decided to include the standard deviation of the samples measured during the whole experiment instead of the relative error for each determination since it is more representative of the inlet and outlet fluid characteristics. The system stationary state regarding coagulant mixing was assessed by the K to Na concentrations ratio in the outlet stream, as it should remain constant even if the source input changes its concentrations by evaporation over the day. The ratio remained almost constant along the whole experiment (1.46 $\pm$ 0.07) indicating no major changes in wastewater coagulation process along the operation time. Also, as seen in Table 4, Na and K concentrations presented less than 4% standard deviation, consistent with no significant changes in the inlet wastewater characteristics. The temperature was stable during the entire operation being around 13.3 $\pm$ 0.5 °C. Despite low alkalinity, good pH control was achieved, proving the efficiency of using a static mixer instead of a stirred tank for promoting the continuous flocculation under field conditions.

Table 5 shows the nitrogen, phosphorous and organic matter concentrations before and after the coagulation-flocculation-sedimentation system. Results evidenced the removal of most of the particulate and precipitable elements. Turbidity exhibited the highest removal with 99.7% average, showing almost complete removal of suspended solids (SS), corresponding its value (3.4 NTU) to a concentration of approximately 5 mg L^{-1} of suspended solids (Rügner et al., 2013). COD and P-Org followed, with 97.8 $\pm$ 1% and 96.0 $\pm$ 9% average removal, respectively, while the TRP was 95.1 $\pm$ 5% (Figure 8). Nitrogen removal was significant only for the organic fraction, being around 68.2 $\pm$ 8%, with low ammonia removal. Nitrite and nitrate were absent. Low standard deviation observed in almost all variables indicated high stability both in the coagulation-flocculation step as in the settler afterwards. Only nitrogen showed more pronounced fluctuations, possibly due to the high initial content and therefore the marked effect caused by occasional small floc losses. Nevertheless, these fluctuations were within the acceptable range, with minor effects over the general performance.

Results obtained agree with those reported in (Okoth et al., 2008), who attained removal efficiencies between 70% to 90% for a lamella settler applied to re-suspended sludge samples from a communal wastewater treatment plant. García et al. (2018) also found similar

Table 2. Comparison of the experimental liquid residence time (τ) and those predicted by CFD.

GEOMETRY	*T* (MIN)		
	CFD	Experimental	% difference
C	19.63 $\pm$ 0.18	19.33 $\pm$ 0.84	1.57%
D	19.77 $\pm$ 0.13	19.96 $\pm$ 0.82	0.96%
E	19.39 $\pm$ 0.17	18.98 $\pm$ 0.83	2.16%

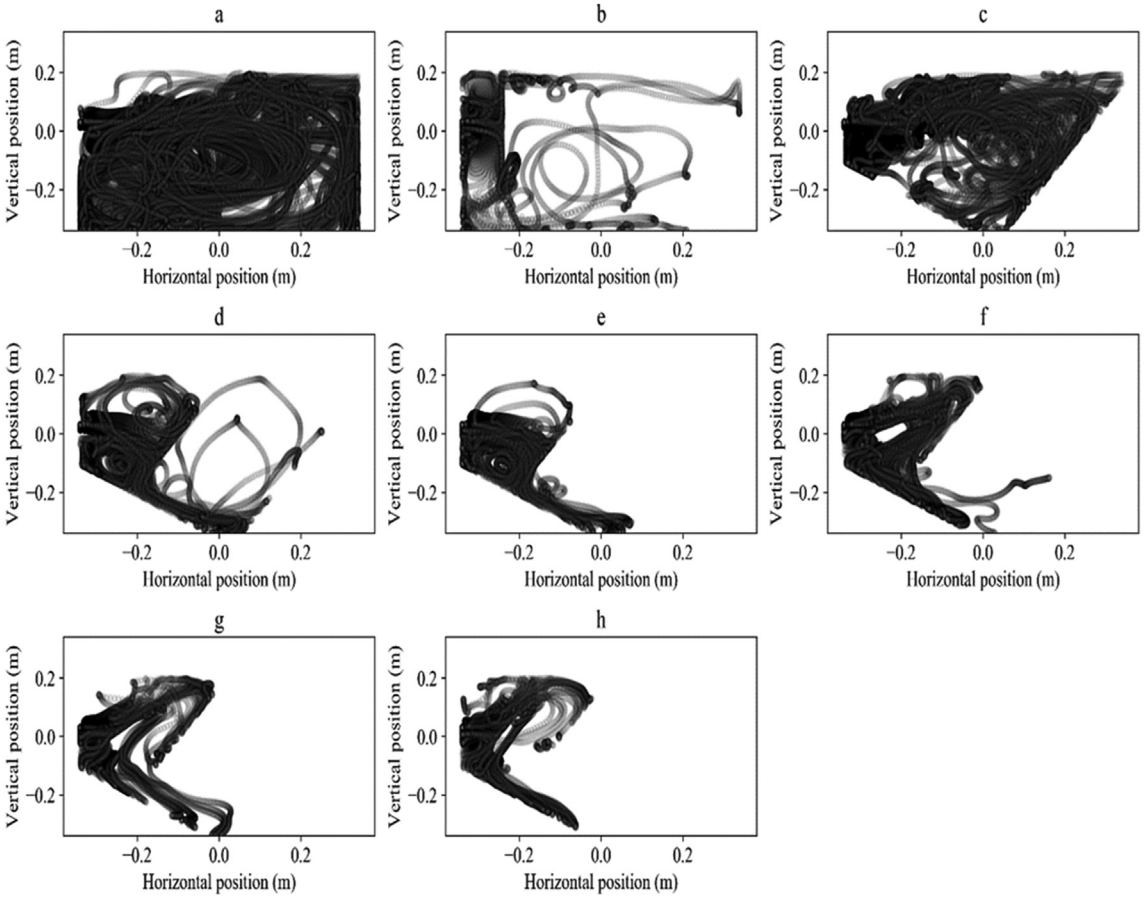

Figure 7. Calculated particles trajectories. Both axes show the x-y position, where the 0,0 corresponds to the center of each geometry. Letters (a–h) correspond to configurations shown in Figure 1.

Table 3. Comparison of the settling efficiency in terms of the indexes α, β and SPI (Eqs. (6), (7), and (8)) obtained from the CFD simulation of 200 inertial particles for the studied geometries. Letters as in Figures 1 and 7.

	A	B	C	D	E	F	G	H
A	0.46	0.82	0.69	0.73	0.84	0.69	0.74	0.73
B	0.72	0.99	0.96	1.00	1.00	1.00	1.00	1.00
SPI%	52.6%	89.4%	81.0%	86.4%	92.1%	84.6%	86.9%	86.5%
S.D.	0.1%	0.3%	0.1%	0.2%	0.2%	0.1%	0.3%	0.2%

S.D.: standard deviation of the *SPI%* as estimated from five simulations of 200 particles trajectories starting from different initial positions.

removal efficiencies for a lamella settler coupled with a microalgae treatment system in a full field scale. In a previous contribution (Fleite et al., 2020), important ammonia removal was found, attributed to volatilization in the mixing step for calcium hydroxide. The absence of ammonia removal in the set-up tested in this work can be related to the use of a second static mixer after hydroxide addition, ensuring a better mixing and a correct pH regulation. Although this entails no ammonia removal, it could be considered an advantage since ammonia is better than nitrite for nitrogen fertigation due to less leaching risk (Delin and Stenberg, 2020). With a convenient dose, nitrogen recycling could be achieved, contributing to production sustainability.

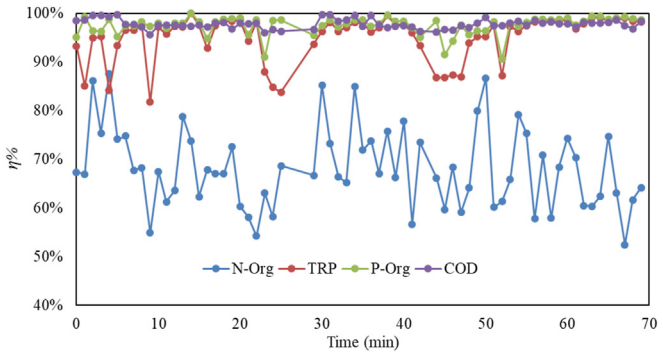

Figure 8. Nutrients and organic matter removal efficiencies as defined in Eq. (9) for a representative period during the continuous field experiment.

Regarding the final disposal of the liquid outlet stream, EC and SAR values obtained (Table 4) would allow the use for irrigation concerning soil stability according to general classifications (Halliwell et al., 2001) although the high potassium content could cause some infiltration problems (Smith et al., 2015). The absence of nitrite and nitrate was also promising as those ions can easily percolate (Ali, 2010) threatening groundwater quality. Even though phosphorous could be of main concern because of its percolation risk (Prior et al., 2009) the attained final concentration was sufficiently low to prevent it (Table 5). Future

Table 4. Concentrations of the main ions and control variables measured before and after the coagulation-flocculation-sedimentation treatment.

		Na^+	K^+	Hardness	Alk	pH	EC	SAR
		mg/L	mg/L	mM	mM	-	mS/cm	$mmol_c/L$
Inlet stream	Mean	81.76	130.92	2.57	10.48	8.45	1.27	3.14
	S.D.	1.6	5.1	0.15	0.45	0.04	0.01	0.15
Outlet stream	Mean	86.93	114.36	12.00	2.63	7.09	3.39	1.54
	S.D.	1.10	1.83	1.21	0.51	0.32	0.38	0.15
Solid concentrated outlet stream	Mean	86.0	129.8	10.20	2.75	7.99	3.00	1.66
	S.D.	2.6	3.1	1.13	1.67	0.03	0.20	0.04

S.D.: standard deviation.

Table 5. Nutrients and organic matter concentrations before and after the settling treatment. Removal efficiency η % as defined in Eq. (9).

		NH4+	N-Org	TRP	P-Org	COD	Turbidity
		mgN/L	mgN/L	mgP/L	mg P/L	mg O_2/L	(NTU)
Inlet stream	Mean	13.93	25.37	22.25	25.02	3370	1179
	S.D.	1.74	2.22	0.76	1.19	318	3.3
Outlet stream	Mean	12.61	8.08	1.08	1.23	73	3.4
	S.D.	1.99	2.10	1.03	1.16	32	0.2
	η%	9.5%	68.2%	95.1%	95.1%	97.8%	99.7%
Solid concentrated outlet stream	Mean	13.94	88.40	-	181.52	14844	-
	S.D.	0.44	0.22	-	0.59	250	-

S.D.: standard deviation.

studies will consider methods such as fertigation (Jaramillo and Restrepo, 2017) together with nutrient management for final disposal of treated waters from feedlot runoff.

3.4.2. Spectroscopic analysis

Table 6 shows the spectral indices and the absorbance at given wavenumbers for the untreated effluent and the liquid leaving the settler in the outflow stream. The absorbance wavelength ratios of the commonly used spectral relations are given in the table between brackets for each index. An increase in the E2/E3 ratio, as the one found, generally indicates a decrease in the average molecular weight of the dissolved organic matter (Zhang et al., 2011). The significant absorbance decrease at wavenumbers associated to aromatic compounds (measured at 272 and 254 nm) and to humic substances (measured at 285 nm) is a clear indicator of organic matter being removed, with the consequent enrichment in more labile organic compounds with lower molecular weight (Waldrip et al., 2014; Zhang et al., 2011).

The E4/E6 ratio, usually related to the molecular weight of humic acids, showed a significant change, which can be interpreted as an increase in the relative content of volatile acids and low molecular weight compounds, with simple aliphatic substitutions (Zhang et al., 2011). This is consistent with the observed change in the E2/E3 ratio, which, as previously mentioned, showed a shift towards substances of lower molecular weight. The E253/E203 ratio pointed to a decrease in the number of polar substitutions in the aromatic rings (Waldrip et al., 2014). This can be related, considering the decrease in aromaticity (measured at 254 nm and 272 nm), and molecular weight (E2/E3), with the enrichment in compounds like salicylic, phthalic and volatile fatty acids, and the decrease in other molecules with higher number of substitutions.

Figures 9 and 10 show the fluorescence excitation-emission matrices (EEM) of the untreated effluent and the liquid collected in the outflow stream, respectively. The colors show the fluorescence intensity in arbitrary units. The untreated wastewater EEM (Figure 9) evidenced peaks and emission regions associated with humic substances (Coble et al., 2014; Peiris et al., 2011). Hence, humic acids and structurally similar molecules would be the main organic fraction of the untreated effluent. A blue shift in fluorescence emission can be observed comparing Figures 9 and 10, indicating a relative increase in low molecular weight substances occasioned by the treatment. This shift can be associated with an increase in the proportion of low molecular weight phenolic organic matter, with a lower degree of substitution in the aromatic rings (Coble et al., 2014; Peiris et al., 2011). The spectral results are consistent with the dynamics of the coagulation process since higher molecular weight molecules are prone to be retained more readily in the solid phase than those with lower molecular weight.

Another important peak observed in the EEMs is the one related to protein-like substances. It typically appears in the region (Ex 270–280 nm/Em 330–360 nm) where tryptophan and similar compounds are found (Coble et al., 2014; Hudson et al., 2007). In the treated wastewater (Figure 10) the peak is marked, while it is only slightly observed in the raw effluent EEM (Figure 9). Probably related molecules in the feedlot wastewater are tryptophan, indol-3-acetic acid (which is formed by microbial oxidation of tryptophan) and similar compounds present in grains (Bandurski and Schulze, 1977). Corn grains (Zea mays), the main food

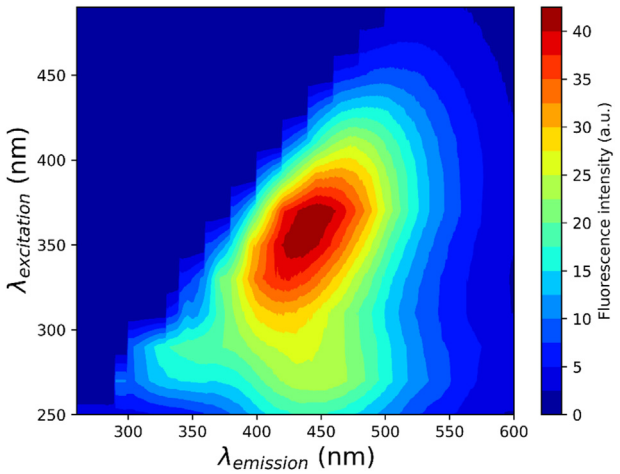

Figure 9. EEM for the untreated wastewater.

Table 6. UV-Vis spectral indexes.

Wastewater	E2/E3 (254/365)	E4/E6 (472/664)	E253/E203	Abs 285 nm	Abs 272 nm	Abs 254 nm
Raw wastewater	1.49 ± 0.01	1.54 ± 0.02	0.86 ± 0.005	1.94 ± 0.05	2.02 ± 0.02	2.11 ± 0.03
Settler Outlet	5.17 ± 0.04	2.58 ± 0.03	0.11 ± 0.01	0.022 ± 0.001	0.026 ± 0.002	0.029 ± 0.001

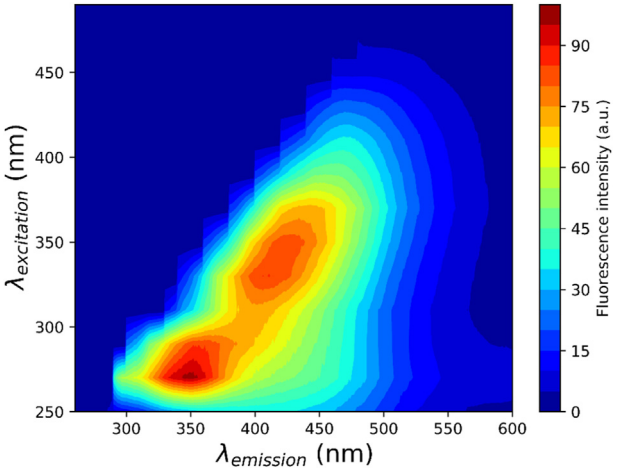

Figure 10. EEM for the treated wastewater.

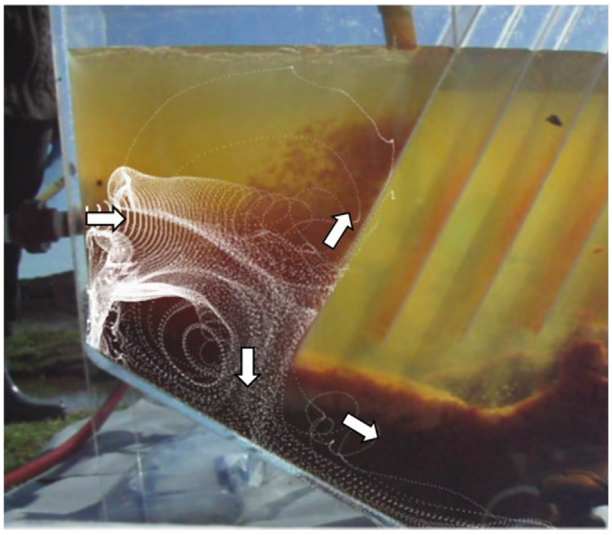

Figure 11. CFD particle trajectories (-e- geometry configuration, Figure 1) superimposed to a photograph of the experimental set-up. White arrows show the main floc flow direction as seen during operation.

source in feedlots in Argentina and worldwide (Moltz et al., 2019; Pordomingo, 2005), have a large amount of these indole-like substances (Bandurski and Schulze, 1977). The presence of these protein-like compounds would explain the lower removal of organic nitrogen in the settler compared to the removal of phosphorus and COD under equal conditions. Thus, organic nitrogen would remain in solution because it is mainly associated with amino acids related compounds. Indole-3-acetic acid and similar molecules are very soluble in water and have a high fluorescence intensity given by the indole group (Coble et al., 2014). The presence of this compound would explain the blue shift in fluorescence observed for the treated wastewater. When humic acids were removed by coagulation-sedimentation, the transmittance increased significantly, and the indole fluorescence became evident.

3.4.3. Floc trajectories in the settler

Finally, the inertial solid particles trajectories obtained by the CFD code (Figure 7 e) were compared with the filmed and photographed inflow flocs during the experimental in-field operation. Figure 11 shows that the simulated motion was in close agreement with floc trajectories. Also, non-reached areas were well predicted by the simulations of the injected particles trajectories. Despite neglecting inter flocs interaction and floc breakage, discrete spherical particles with a setting velocity based on the initial settling velocity from the settling curve resulted in a satisfactory estimation of floc behavior. Therefore, the solid particles motion simulation can help the optimization and, together with the defined *SPI* index, would allow examining alternative settling systems for decreasing wastewater treatment costs.

4. Conclusions

The settling performance of a pilot-scale lamella settler for the continuous treatment of the wastewater contained in a feedlot accumulation pond was examined. The pilot-scale unit used was built based on an optimization of the geometry using CFD simulation carried out with the Gerris flow solver software. It was found that the simulations were able to properly represent experimental results of residence time distributions in the bench-scale unit. Also, it was shown that simulations of the motion of injected inertial particles can provide further insight into the efficiency of the settler for solid separation, thus contributing to the optimization process.

The settler was tested in continuous operation in the field. The system was very efficient for removing suspended solids, organic matter and phosphorus. The resulting clarified liquid was characterized to get insights in the remaining species, mainly those related to the organic nitrogen, which was only partially removed. The proposed system is easy-to-use and affordable. It would be an efficient option for small and large feedlots to treat wastewaters. In order to assess its long-term functionality, the prototype provided with automatization and control systems will be mounted in an establishment to test the continuous function for days and under different periods of the year. In addition, there is ongoing research to assess the use of the solid and the liquid as sub-products: the liquid for fertigation and the solid as a fertilizer. In the end, it is expected to develop a system that can be commercialized for the use in small establishments with recommendations for the users.

Declarations

Author contribution statement

Santiago N. Fleite: Conceived and designed the experiments; Performed the experiments; Analyzed and interpreted the data; Wrote the paper.

Ana R. García, M. Gabriela Lagorio: Analyzed and interpreted the data; Contributed reagents, materials, analysis tools or data.

Christian De los Santos: Performed the experiments.

Leandro L. Missoni: Analyzed and interpreted the data.

Rocío Torres: Performed the experiments; Analyzed and interpreted the data.

Miryan Cassanello: Conceived and designed the experiments; Analyzed and interpreted the data; Contributed reagents, materials, analysis tools or data; Wrote the paper.

Funding statement

This work was supported by CONICET (PIP 1122015-0100902CO) and Universidad de Buenos Aires (UBACyT 20020170100604BA, UBACyT 20020150100156BA and UBACyT20020170100037BA). MGL and MC are Research Members of CONICET (Argentina). SF and RT are CONICET scholarship holders.

Data availability statement

Data will be made available on request.

Declaration of interests statement

The authors declare no conflict of interest.

Additional information

No additional information is available for this paper.

Acknowledgements

We would also like to thank Dr. M. Maestri for his help and support.

References

Al-Sammarraee, M., Chan, A., Salim, S.M., Mahabaleswar, U.S., 2009. Large-eddy simulations of particle sedimentation in a longitudinal sedimentation basin of a water treatment plant. Part I: particle settling performance. Chem. Eng. J. 152 (2–3), 307–314.

Ali, M.H., 2010. Pollution of water resources from agricultural fields and its control. In: Practices of Irrigation & On-Farm Water Management, 2. Springer, New York, pp. 241–269.

APHA, 2017. Standard Methods for the Examination of Water and Wastewater. American Public Health Association, Washington, DC.

Arendze, S., Sibiya, M.S., 2016. Comparing the flow dynamics and particle settling in full-scale sedimentation tanks of different lengths. Water Supply 17 (4), 998–1006.

Bandurski, R.S., Schulze, A., 1977. Concentration of indole-3-acetic acid and its derivatives in plants. Plant Physiol. 60 (2), 211–213.

Brown Phillip, P., Lawler Desmond, F., 2003. Sphere drag and settling velocity revisited. J. Environ. Eng. 129 (3), 222–231.

Ciapparelli, I.C., de Iorio, A.F., García, A.R., 2016. Phosphorus downward movement in soil highly charged with cattle manure. Environ. Earth Sci. 75 (7), 568–578.

Coble, P.G., Lead, J., Baker, A., Reynolds, D.M., Spencer, R.G.M., 2014. Aquatic Organic Matter Fluorescence. Cambridge University Press.

Delin, S., Stenberg, M., 2020. Effects on Nitrate Leaching of the Timing of Cattle Slurry Application to Leys. Soil Use and Management.

Fettig, J., Pick, V., Liebe, H., 2017. Particle separation from road runoff by a decentralised lamella system laboratory tests and experiences in the field. Water Sci. Technol. 75 (9), 2056–2063.

Fleite, S.N., García, A.R., los Santos, C. N. De, de Iorio, A.F., Cassanello, M., 2020. Static mixer continuous chemical coagulation-flocculation for cattle feedlot wastewater treatment. Desalination And Water Treatment 189, 98–107.

Fuchs, S., Mayer, I., Haller, B., Roth, H., 2013. Lamella settlers for storm water treatment - performance and design recommendations. Water Sci. Technol. 69 (2), 278–285.

García, Ana R., Maisonnave, R., Massobrio, M.J., de Iorio, A.R.F., 2012. Field-scale evaluation of water fluxes and manure solution leaching in feedlot pen soils. J. Environ. Qual. 41 (5), 1591–1599.

García, A.R., Fleite, S.N., Pugliese, D.V., de Iorio, A.F., 2013. Feedlots and pollution-A growing threat to water resources of agro-production zone in Argentina. Environ. Sci. Technol. 47 (21), 11932–11933.

García, J., Ortiz, A., Álvarez, E., Belohlav, V., García-Galán, M.J., Díez-Montero, R., Álvarez, J.A., Uggetti, E., 2018. Nutrient removal from agricultural run-off in demonstrative full scale tubular photobioreactors for microalgae growth. Ecol. Eng. 120, 513–521.

Getaz, M., 2018. Lamella clarifiers in sugar processing. Int. Sugar J. 120 (1438), 770–776.

Guo, C.Q., Dong, B., Liu, J.J., Liu, F.P., 2015. The best indicator of hydraulic short-circuiting and mixing of constructed wetlands. Water Pract. Technol. 10 (3), 505–516.

Halliwell, D.J., Barlow, K.M., Nash, D.M., 2001. A review of the effects of wastewater sodium on soil physical properties and their implications for irrigation systems. Soil Res. 39 (6), 1259.

He, W., Xue, L., Gorczyca, B., Nan, J., Shi, Z., 2018. Experimental and CFD studies of floc growth dependence on baffle width in square stirred-tank reactors for flocculation. Separ. Purif. Technol. 190, 228–242.

Hjorth, M., Christensen, K.V., Christensen, M.L., Sommer, S.G., 2010. Solid–liquid separation of animal slurry in theory and practice. A review. *Agronomy for Sustainable Development* 30 (1), 153–180.

Hudson, N., Baker, A., Reynolds, D., 2007. Fluorescence analysis of dissolved organic matter in natural, waste and polluted waters—a review. River Res. Appl. 23 (6), 631–649.

Jahne, M.A., Rogers, S.W., Ramler, I.P., Holder, E., Hayes, G., 2014. Hierarchal clustering yields insight into multidrug-resistant bacteria isolated from a cattle feedlot wastewater treatment system. Environ. Monit. Assess. 187 (1), 4168.

Jaramillo María, F., Restrepo, I., 2017. Wastewater reuse in agriculture: a review about its limitations and benefits. Sustainability 9 (10), 1734.

Keen, T.R., Campbell, T.J., Dykes, J.D., Martin, P.J., 2013. Gerris Flow Solver: Implementation and Application. Defense Technical Information Center.

Lagrée, P.-Y., Staron, L., Popinet, S., 2011. The granular column collapse as a continuum: validity of a two-dimensional Navier-Stokes model with a {μ} (I)-rheology. J. Fluid Mech. 686, 378–408.

Martín-Rilo, S., Coimbra, R.N., Martín-Villacorta, J., Otero, M., 2015. Treatment of dairy industry wastewater by oxygen injection: performance and outlay parameters from the full scale implementation. J. Clean. Prod. 86, 15–23.

Menges, F., 2020. Spectragryph-optical Spectroscopy Software, 1, pp. 2016–2017. Version 1.2.14. http://www.effemm2.de/spectragryph/.

Moltz, B., Yu, M., Osei, E., Smith, W.B., Poe, B., 2019. The economic analysis of corn grain optimization and price variation for cattle on feed in Texas. Agriculture 9 (7), 159.

Ohno, T., He, Z., 2011. Fluorescence Spectroscopic Analysis of Organic Matter Fractions: the Current Status and a Tutorial Case Study. Environmental Chemistry of Animal Manure. Nova Science, New York, pp. 83–103.

Okoth, G., Centikaya, S., Brüggemann, J., Thöming, J., 2008. On hydrodynamic optimisation of multi-channel counter-flow lamella settlers and separation efficiency of cohesive particles. Chem. Eng. Process: Process Intensification 47 (1), 90–100.

O'Callaghan, J., Rickard, G., Popinet, S., Stevens, C., 2010. Response of buoyant plumes to transient discharges investigated using an adaptive solver. J. Geophys. Res.: Oceans 115 (C11).

Peiris, R.H., Budman, H., Moresoli, C., Legge, R.L., 2011. Identification of humic acid-like and fulvic acid-like natural organic matter in river water using fluorescence spectroscopy. Water Sci. Technol. 63 (10), 2427–2433.

Pepple, M., Andersen, L.,S., Burns, D.,T., Moody, B., 2011. Physical and chemical properties of runoff effluent from beef feedlots in Iowa. Transactions of the ASABE 54 (3), 1079–1084.

Popinet, S., 2003. Gerris: a tree-based adaptive solver for the incompressible Euler equations in complex geometries. J. Comput. Phys. 190 (2), 572–600.

Pordomingo, A.J., 2005. *Feedlot: Alimentación, Diseño Y Manejo*. INTA-EEA Anguil. https://inta.gob.ar/sites/default/files/script-tmp-inta_feedlot_2013.pdf.

Prior, M., Smanhoto, A., Sampaio, S., Nobrega, L., Opazo, M., Dieter, J., 2009. Accumulation and percolation of phosphorus in the soil due to the application of wastewater from swine farming in maize culture (Zea mays L.). Appl. Res. Agrotechnol. 2 (1).

Rügner, H., Schwientek, M., Beckingham, B., Kuch, B., Grathwohl, P., 2013. Turbidity as a proxy for total suspended solids (TSS) and particle facilitated pollutant transport in catchments. Environ. Earth Sci. 69 (2), 373–380.

Salem, A.I., Okoth, G., Thöming, J., 2011. An approach to improve the separation of solid–liquid suspensions in inclined plate settlers: CFD simulation and experimental validation. Water Res. 45 (11), 3541–3549.

Salvador, F.J., Romero, J.-V., Roselló, M.-D., Jaramillo, D., 2016. Numerical simulation of primary atomization in diesel spray at low injection pressure. J. Comput. Appl. Math. 291, 94–102.

Shen, Y., Yanagimachi, K., 2011. CFD-aided cell settler design optimization and scale-up: effect of geometric design and operational variables on separation performance. Biotechnol. Prog. 27 (5), 1282–1296.

Shui, P., Valluri, P., Popinet, S., Govindarajan, R., 2015. Direct numerical simulation study of hydrodynamic interactions between immersed solids and wall during flow. Procedia IUTAM 15, 150–157.

Smith, C.J., Oster, J.D., Sposito, G., 2015. Potassium and magnesium in irrigation water quality assessment. Agric. Water Manag. 157, 59–64.

Takata, K., Kurose, R., 2017. Influence of density flow on treated water turbidity in a sedimentation basin with inclined plate settler. Water Supply 17 (4), 1140–1148.

Tarpagkou, R., Pantokratoras, A., 2014. The influence of lamellar settler in sedimentation tanks for potable water treatment — a computational fluid dynamic study. Powder Technol. 268, 139–149.

Tchobanoglous, G., Stensel, H., Tsuchihashi, R., Burton, F., Abu-Orf, M., Bowden, G., Pfrang, W., 2014a. Metcalf and Eddy, Wastewater Engineering: Treatment, Reuse and Recovery, fifth ed. McGraw Hill.

Tchobanoglous, G., Stensel, H.D., Tsuchihashi, R., Burton, F., Abu-Orf, M., Bowden, G., Pfrang, W., 2014b. Waterwater Engineering: Treatment and Resource Recovery. *Metcalf and Eddy Inc*. McGraw-Hill, New York.

Teixeira, E.C., do Nascimento Siqueira, R., 2008. Performance assessment of hydraulic efficiency indexes. J. Environ. Eng. 134 (10), 851–859.

Tomar, G., Fuster, D., Zaleski, S., Popinet, S., 2010. Multiscale simulations of primary atomization. Comput. Fluids 39 (10), 1864–1874.

Tsai, D.D.-W., Ramaraj, R., Chen, P.H., 2012. A method of short-circuiting comparison. Water Resour. Manag. 26 (9), 2689–2702.

Vahidifar, S., Saffarian, M.R., Hajidavalloo, E., 2018. Introducing the theory of successful settling in order to evaluate and optimize the sedimentation tanks. Meccanica 53 (14), 3477–3493.

Wahl, M.D., Brown, L.C., Soboyejo, A.O., Martin, J., Dong, B., 2010. Quantifying the hydraulic performance of treatment wetlands using the moment index. Ecol. Eng. 36 (12), 1691–1699.

Waldrip, H.M., He, Z., Todd, R.W., Hunt, J.F., Rhoades, M.B., Cole, N.A., 2014. Characterization of organic matter in beef feedyard manure by ultraviolet-visible and fourier transform infrared spectroscopies. J. Environ. Qual. 43 (2), 690–700.

Weiss, G., 2013. Innovative use of lamella clarifiers for central stormwater treatment in separate sewer systems. Water Sci. Technol. 69 (8), 1606–1611.
Wilson, J.M., Venayagamoorthy, S.K., 2010. Evaluation of hydraulic efficiency of disinfection systems based on residence time distribution curves. Environ. Sci. Technol. 44 (24), 9377–9382.
Xue, J., Guo, B., Gong, Z., 2018. Physico-chemical processes. Water Environ. Res. 90 (10), 1392–1438.
Zhang, M., He, Z., Zhao, A., 2011. In: He, Z. (Ed.), Environmental Chemistry of Animal Manure. Nova Science Publishers, Inc, pp. 61–81.